THE JOURNAL OF PHYSICAL CHEMISTRY Letters

Letter

pubs.acs.org/JPCL

Investigating Superoxide Transfer through a μ-1,2-O_2 Bridge between Nonheme Ni^{III}–Peroxo and Mn^{II} Species by DFT Methods to Bridge Theoretical and Experimental Views

Kyung-Bin Cho,[†] Jaeheung Cho,[‡] Sason Shaik,[#] and Wonwoo Nam*[,†]

[†]Department of Chemistry and Nano Science, Ewha Womans University, 120-750 Seoul, Korea

[‡]Department of Emerging Materials Science, DGIST, 711-873 Daegu, Korea

[#]Institute of Chemistry and the Lise Meitner-Minerva Center for Computational Quantum Chemistry, The Hebrew University of Jerusalem, 91904 Jerusalem, Israel

Supporting Information

ABSTRACT: Previously, a fast unprecedented $O_2^{\bullet-}$ transfer reaction has been observed experimentally when adding a Mn^{II} complex into a solution containing a Ni^{III}–peroxo complex. Due to the fast reaction rate, no intermediates were observed. We have investigated this reaction with density functional theory (DFT) and show that DFT is unusually problematic in reproducing the correct spin state for the investigated Ni^{III}–peroxo complex, something which calls for examination of all previous Ni–dioxygen studies. Surprisingly, the BP86 functional is shown to yield energies more in agreement with known experiments than B3LYP. The calculations reveal for the first time an intermediate structure in a complete $O_2^{\bullet-}$ transfer reaction, shown here to be a short-lived bridging Ni-(μ-1,2-O_2)-Mn structure.

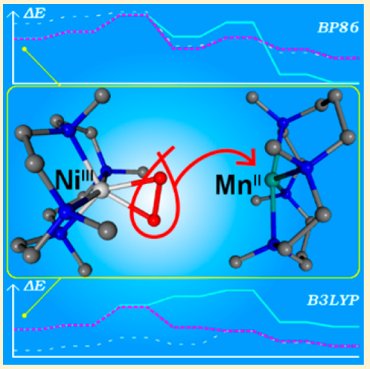

SECTION: Molecular Structure, Quantum Chemistry, and General Theory

Dioxygen (O_2) interactions with metalloenzymes are common reactions in nature.[1−12] To study and advance the knowledge about these reactions, many biomimetic models have been synthesized over the years that vary in composition, structure, and purpose.[13−16] As part of this knowledge base, our laboratory in collaboration with others previously synthesized and characterized both an end-on (η^1) $[(14\text{-TMC})Ni^{II}O_2]^+$ species (14-TMC = 1,4,8,11-tetramethyl-1,4,8,11-tetraazacyclotetradecane)[17] and a side-on (η^2) $[(12\text{-TMC})Ni^{III}O_2]^+$ species (**1**, 12-TMC = 1,4,7,10-tetramethyl-1,4,7,10-tetraazacyclododecane).[18] In the latter study, we also observed a complete intermolecular superoxo ($O_2^{\bullet-}$) transfer reaction occurring when adding $[(14\text{-TMC})Mn^{II}]^{2+}$ (**2**) to **1**. This unprecedented reaction occurred rapidly without buildup of any intermediates, even at −50 °C. The reaction was proposed to go through a bimolecular mechanism based on kinetic analysis, but the exact structure of any potential intermediates remains unknown. Such potential intermediates may well be MO_2M' structures in which O_2 bridges two transition metals (M and M′). Indeed, related stable bridging structures between metals that have been characterized to date are diverse in type (e.g., bis-μ-oxo,[19,20] μ-1,2-peroxo,[21,22] μ-η^2:η^2-peroxo[22,23]). The existence of these complexes implies that the observed $O_2^{\bullet-}$ transfer may occur with an intermediate. Furthermore, a complete $O_2^{\bullet-}$ transfer was also observed when replacing the Ni complex with Co complexes.[16] Therefore, elucidation of the reaction mechanism for the current study may set a precedence to future studies.

Due to the fast reaction rate, a theoretical approach would be suitable, as implied in the previous study.[18] However, previous theoretical studies on Ni^{III}–peroxo and/or Ni^{II}–superoxo systems revealed that a theoretical study is also not straightforward and requires a great deal of caution. For instance, density functional theory (DFT)[24] calculations on $[(14\text{-TMC})NiO_2]^+$ yielded the quartet multiplicity as the ground state.[17,25] These studies used BP86[26−28] or B3LYP[26,29−31] functionals, and others were also tested with the same results.[25] This was in contrast to EPR experiments assigning this species to a doublet multiplicity,[17] as was done later in the related $[(13\text{-TMC})NiO_2]^+$ species.[32] This issue was addressed in an ab initio study[33] using the CASSCF method,[34] which also gave the quartet as the ground state. This prompted the authors to point out the deficiencies of the EPR results as a possible reason for the discrepancy.[33] However, the CASSCF calculations indeed gave the doublet state as the ground state for **1**, in agreement with experiments that found it to be in the S = 1/2 state by the ^{1}H NMR Evans method.[18] Even so, the study took issue with the description of **1** as a Ni^{III}–peroxo species and instead advocated a Ni^{II}–superoxo description.

Received: June 11, 2014
Accepted: June 26, 2014

   dx.doi.org/10.1021/jz501193k | J. Phys. Chem. Lett. 2014, 5, 2437−2442

Table 1. Energy Difference $\Delta E = {}^4E - {}^2E$ for Different DFT Functionals in kcal/mol[a]

CASSCF[b]	B3LYP	BP86[c]	BP86[d]	BLYP	OPBE	OLYP	B3P86	PBE0	B3LYP*	CAM-B3LYP
4.6	−6.91	1.90	2.66	1.11	−3.43	−3.64	−5.79	−7.76	−2.99	−7.34

[a]The energies are calculated with the TZVP basis set with geometries fully optimized in the gas phase with the indicated functional. [b]CASSCF(7,5) values taken from ref 33. [c]BP86 using the VWN5 local correlational functional, named BVP86 in Gaussian 09.[36] [d]BP86 using the Perdew local correlational functional.[27]

Table 2. Selected Distances in Ångströms.[a]

	Ni−O1	Ni−O2	O1−O2	Ni−N1	Ni−N2	Ni−N3	Ni−N4	RMSD[b]
X-ray[c]	1.89	1.88	1.39	2.16	2.16	2.03	2.04	0.00
				BP86/SVP				
doublet	**1.89**	**1.89**	**1.39**	2.21	2.21	2.06	2.06	0.22
quartet	2.06	2.06	1.33	2.18	2.18	2.13	2.13	0.23
				BP86/TZVP				
doublet	**1.89**	**1.89**	1.40	2.21	2.21	**2.05**	**2.05**	0.21
quartet	2.07	2.07	1.34	**2.17**	**2.17**	2.12	2.12	0.22
				B3LYP/SVP				
doublet	1.95	1.95	1.35	2.21	2.21	2.09	2.09	**0.20**
quartet	2.07	2.07	1.32	2.20	2.20	2.14	2.14	0.22

[a]Best fits to the X-ray structure are shown in bold. [b]RMSD to the X-ray structure. [c]Values taken from ref 18.

Therefore, it is clear that there may also be a theoretical problem to decipher a reliable theoretical methodology, which must be carefully evaluated against known experiments. In this study, we investigate the intriguing $O_2^{\bullet-}$ transfer reaction mechanism between **1** and **2**, leading to the formation of $[(12\text{-TMC})Ni^{II}]^{2+}$ (**3**) and $[(14\text{-TMC})Mn^{III}O_2]^{+}$ (**4**). As ab initio calculations are not feasible for reaction mechanism studies, we chose DFT after some careful investigations into its validity for the current system. The aim of this study is two-fold, (1) to aid the experimentalists by unraveling a possible reaction mechanism of the $O_2^{\bullet-}$ transfer reaction between **1** and **2** and (2) to aid the theoreticians by carefully evaluating the applicability of DFT functionals (primarily BP86 and B3LYP) for Ni^{III}−peroxo/Ni^{II}−superoxo systems.

Energy Accuracy of DFT. As mentioned above, earlier experimental studies have implicated a doublet ground state for **1**,[18] and CASSCF ab initio studies also have shown that the doublet state is preferred by 4.6/6.3 kcal/mol (depending on the choice of active space).[33] We have tested a range of functionals in combination with different basis sets and models against this benchmark test. For instance, Table 1 shows the energy difference between the quartet and doublet states using 10 different DFT functionals optimized with TZVP basis set (see also Table S1, Supporting Information). As can be seen, only the pure functionals BP86 (two versions; see the Methods section) and BLYP give a positive ${}^4E - {}^2E$ difference (i.e., the doublet is lower in energy). Remarkably, the widely used B3LYP shows that the doublet is 6.9 kcal/mol higher in energy than the quartet, confirming its occasional bias for high spin states. This value is a whopping 8.8 kcal/mol different from, for instance, BP86 results and 11.5 kcal/mol from the nearest CASSCF results. The spin state preference for B3LYP does not change even after (1) adding solvation, (2) using different basis sets, (3) calculating the free energies, and/or (4) adding a $[ClO_4]^-$ counterion (Tables S1 and S2, Supporting Information). Hence, **1** seems to be a system where BP86 gives the correct spin state ordering while B3LYP and other popular functionals, e.g., PBE0 or OPBE, do not. While this is unusual, it is not unheard of. For **2**, both BP86/Def2-TZVPP//BP86/SVP and B3LYP/Def2-TZVPP//BP86/SVP methods give the sextet as the preferred spin state, in agreement with previous EPR measurements.[35] Therefore, no further tests for **2** were deemed necessary.

Geometrical Accuracy of DFT. As the quality of the optimized geometries is generally known to be less sensitive to functionals and basis sets, we have chosen to compare only three functional/basis set combinations, BP86/SVP, BP86/TZVP, and B3LYP/SVP. The differences in the overall root-mean-square deviations (RMSDs) between the calculated and X-ray structures of **1** are within 0.03 Å (Table 2), with the best fit for the B3LYP/SVP calculated structure. However, this best fit is mainly due to the positions of the peripheral ligand atoms. Looking at seven key bond distances in the core, it becomes clear that the best fit in this region comes from BP86/TZVP doublet calculations (Table 2, bold), in agreement with experiments showing a doublet ground state.[18] However, the differences in these bond lengths and RMSDs between the BP86/SVP and BP86/TZVP doublet calculations are within round-off errors (0.01 Å). Considering the small differences in these bond lengths and RMSDs and that BP86/SVP is less time-consuming than the other two methods, we chose this as our optimization level for further investigations.

On the basis of our above energy and geometry tests, the conclusion is that DFT calculations at the BP86/Def2-TZVPP//BP86/SVP level are likely to yield acceptable results for the $O_2^{\bullet-}$ transfer reaction. However, as B3LYP is (sometimes without tests) widely used in DFT today, we also present the B3LYP/Def2-TZVPP//BP86/SVP energies as there should be an interest in evaluating the performance of the B3LYP functional in the current system as well.

Electronic Structure of 1. Experiments have characterized this structure as a Ni^{III}−peroxo species based on resonance Raman, X-ray structure bond lengths, K-edge X-ray absorption spectra, EXAFS, and DFT calculations.[18] However, ab initio CASSCF in combination with difference dedicated configuration interaction (DDCI) methods has characterized this structure as a Ni^{II}−superoxo species. The theoretical results were interpreted as showing one of the π^* orbitals of O_2 antiferromagnetically coupled to a triplet Ni, prompting the authors to question the experimental interpretations as the

dx.doi.org/10.1021/jz501193k | J. Phys. Chem. Lett. 2014, 5, 2437−2442

resonance Raman frequencies and X-ray structure bond lengths were perceived inconclusive.[33] Indeed, our DFT results are somewhat similar to the CASSCF results, but because the Mulliken spin density distribution on O_2 is only 0.10/0.48 (BP86/B3LYP, respectively) and not −1, as would be expected for an antiferromagnetic coupling to a superoxide radical (Tables S7 and S8 for doublet **1**, Supporting Information), our result is a better fit to the interpretation that a combined bonding Ni 3d−O_2 π^* orbital is formed containing one electron from each side coupled together in the same orbital. Orbital analysis confirm this view as only one singly occupied orbital (instead of three) is found. Also note that the corresponding Mulliken spin density distribution on Ni is 1.08/1.21. Hence, the spin density distribution on the Ni−O_2 moiety is in fact exactly the same spin density distribution that would be seen by EPR on a Ni^{III}−peroxo species. Therefore, the characterization of the compound as Ni^{II}−superoxo or Ni^{III}−-peroxo species would depend on whether one considers the distribution of electrons or the distribution of unpaired electrons. The former is easily deduced from calculations, and the latter is more relevant to spectroscopy. A similar reasoning was recently made for $[(14\text{-TMC})CrO_2]^{2+}$ species.[37]

$O_2^{\bullet-}$ Transfer Reaction. The $O_2^{\bullet-}$ transfer reaction is found to start from a reactant complex (**RC**) via a transition state (**TS1**) to an intermediate **INT** with a bridging μ-1,2-O_2 structure between Ni and Mn (Figure 1). Attempts were done to obtain

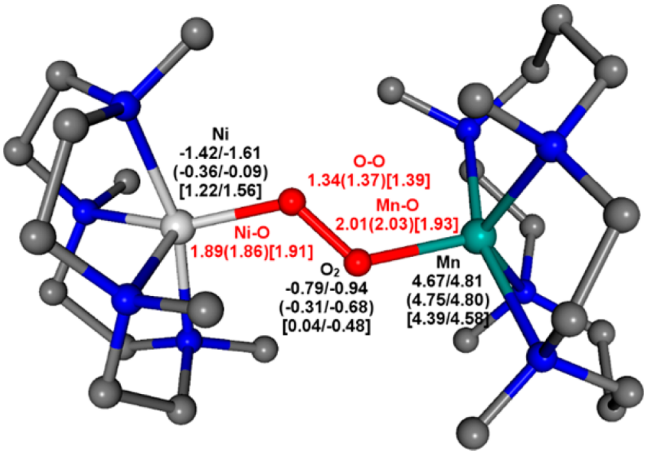

Figure 1. Intermediate structure $^{3(5)[7]}$**INT**, where hydrogen atoms are omitted for clarity. Selected distances (red text, in Ångström) and the Mulliken spin density distribution (black text, BP86/B3LYP) are indicated for triplet(quintet)[septet] states, respectively. Atom colors are white (Ni), turquoise (Mn), red (O), blue (N), and gray (C).

a diamond core bridge (i.e., μ-η^2:η^2-O_2) by partly frozen stepwise optimizations, but ultimately, a μ-1,2-O_2 structure was still obtained. In the second step of the reaction, the Ni−O_2 bond is broken via a transition state **TS2**, and the products **3** and **4** are formed at the product stage (**P**).

The reaction can be mediated through multiple spin states. For instance, the two possible spin states for **1** (doublet and quartet) can combine with the likely spin state of **2** (sextet) either ferromagnetically or antiferromagnetically at the **RC**. This creates a ladder of combined spin states that theoretically ranges from triplet to nonet. However, the nonet state is not attainable at the product stage **P** considering that the highest combined spin state for **3** (singlet or triplet) and **4** (quintet) is a septet. Therefore, the reaction was investigated in the three most likely spin states, triplet, quintet, and septet. It is worth noting that the compounds **1** and **2** in the **RC**, as well as **3** and **4** in **P**, can couple either ferromagnetically or antiferromagnetically between the Ni and Mn centers. However, if these couplings are weak, they will create energy degeneracies along the reaction. At te **RC**, doublet **1** weakly couples (anti)-ferromagnetically to a sextet **2**, resulting in quintet or septet states that are energetically degenerate. At **P**, triplet **3** couples to quintet **4**, creating the degenerate triplet−septet states. The calculated energies are depicted in Figure 2. We henceforth use the left side superscript to indicate multiplicity, where appropriate.

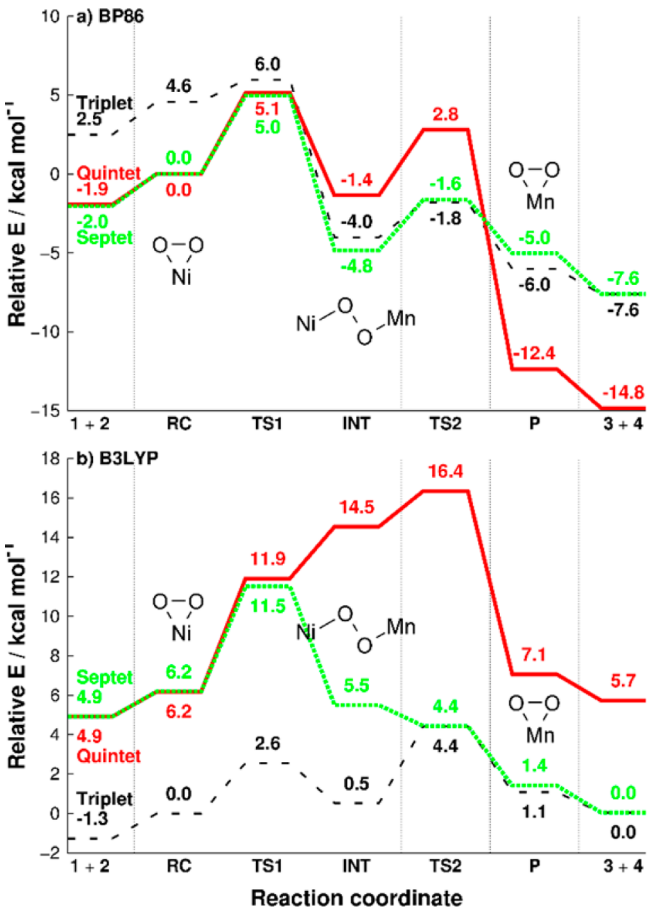

Figure 2. Reaction energy pathway calculated at (a) the BP86/Def2-TZVPP//BP86/SVP level and (b) the B3LYP/Def2-TZVPP//BP86/SVP level.

BP86 Results. The energetically lowest spin states at the **RC** are the degenerate quintet and septet states. In these states, the complexation energy forming the reactant complex $^{5/7}$**RC** was found to be slightly endothermic, about 2 kcal/mol, which will add to the rate-limiting barrier. This value may not be very accurate as dispersion and entropy effects (not included, see the Methods section in the Supporting Information) can be very large during complexations. However, as the rate-limiting barrier is low (vide infra), this will unlikely affect the feasibility of the reaction. The energy degeneracy is kept at $^{5/7}$**TS1**, where the energies are 5.0 (septet) and 5.1 (quintet) kcal/mol, which are also the rate-limiting barriers for this $O_2^{\bullet-}$ transfer reaction as a whole. The degeneracy however splits up at **INT**. The septet state becomes lowest in energy at this stage (at −4.8

dx.doi.org/10.1021/jz501193k | J. Phys. Chem. Lett. 2014, 5, 2437−2442

kcal/mol relative to $^{5/7}$**RC**), and the reaction continues through ^{7}**TS2** (−1.6 kcal/mol) to ^{7}**P** (−5.0 kcal/mol). The quintet state meanwhile leads to a high-energy species ^{5}**INT** (−1.4 kcal/mol), which goes over a high ^{5}**TS2** (2.8 kcal/mol), but becomes a low-energy ^{5}**P** (−12.4 kcal/mol). Due to the relatively high energies at ^{5}**INT** and ^{5}**TS2**, the quintet is unlikely to mediate the reaction at these stages, but it is possible that spin relaxation at the end of the reaction allows ^{5}**P** to be attained.

The triplet state, which is nascent from the high-energy ^{4}**1** antiferromagnetically coupled to ^{6}**2**, is 4.6 kcal/mol higher in energy at **RC**. The reaction occurs over ^{3}**TS1** at 6.0 kcal/mol, and the energy degeneracy with the septet starts to be noticeable at ^{3}**INT** (−4.0 kcal/mol). There is a very small antiferromagnetic effect, causing ^{3}**TS2** to be nominally lowest at −1.8 kcal/mol, and the reaction continues on to ^{3}**P** (−6.0 kcal/mol). The dissociation of **P** into its constituting compounds (**3** and **4**) is found to be on the order of 2 kcal/mol exothermic in all of the spin states, providing some extra driving force to the reaction.

A closer look at the Mulliken spin density distribution for **INT** reveals the character of this transfer (Table S7, Supporting Information). For the energetically lowest species (^{7}**INT**), the combined (Ni + 4 × N) spin is 1.57, which is closest to the high-spin Ni^{II}. The O_2 itself has a peroxide character (0.04), while a spin density of 4.28 on (Mn + 4 × N) implies a Mn^{III} spin. Because the system is in its septet state, no possibilities for antiferromagnetic coupling exist that can complicate the analysis. Hence, roughly one electron can be seen to "shift" from Mn^{II} to the dioxygen moiety to form this intermediate.

B3LYP Results. The complexation energy between **1** and **2** is endothermic here as well (1.3 kcal/mol in all spin states). As described above, the preferred ground state of **1** is a quartet according to B3LYP. Antiferromagnetic coupling between ^{4}**1** and ^{6}**2** at **RC** results in an overall triplet ground state 6.2 kcal/mol lower than the quintet−septet degenerate pair. In fact, the triplet preference is kept for the duration of this reaction, with the initial transition state ^{3}**TS1** being at 2.6 kcal/mol, and at ^{3}**INT**, it is 0.5 kcal/mol above ^{3}**RC**. Because ^{3}**TS2** in the next step is at 4.4 kcal/mol, it also constitutes the rate-limiting value for the whole reaction. The energy at ^{3}**P** is 1.1 kcal/mol, showing that the whole reaction is endothermic according to B3LYP. Even accounting for a couple of kcal/mol in dissociation energies, the reaction is at best thermoneutral.

The degenerate quintet−septet pair passes by their first barriers at 11.5 (^{7}**TS1**) and 11.9 (^{5}**TS1**) kcal/mol, but these states show different behaviors for the rest of the reaction. The quintet state leads to a high-energy ^{5}**INT** at 14.5 kcal/mol, which is in fact energetically higher than its own ^{5}**TS1**. This indicates that there is no stable ^{5}**INT** at this spin state, and the whole of the reaction occurs in one step. Considering that ^{5}**TS2** is even higher in energy (16.4 kcal/mol), this state is ruled out as the mediating spin state. The septet state, while being 5.0 kcal/mol higher in energy than the triplet at **INT**, becomes degenerate with the triplet at ^{7}**TS2** and ^{7}**P** due to the weak (anti)ferromagnetic coupling described above. A stable ^{7}**INT** is not found in this spin state either as ^{7}**TS2** is lower in energy than ^{7}**INT**. At **P**, due to the B3LYP bias for the high-spin ^{3}**3**, the degenerate ^{3}**P**/^{7}**P** pair is lower in energy than ^{5}**P**. The Mulliken spin density distribution for ^{3}**INT** (Table S8, Supporting Information) is −1.93/−0.95/4.82 for (Ni + 4 × N)/O_2/(Mn + 4 × N), respectively, implying a Ni^{II}−superoxo−Mn^{II} species. This is supported by orbital analysis, which clearly shows eight singly occupied orbitals (five α 3d on Mn, two β 3d on Ni, and one β π^* on O_2).

Despite the apparent discrepancy between the different functionals, there are some interesting features that can be drawn from this study. The values of the spin state energy differences for **1**, **2**, **3**, and **4** all differ significantly between BP86 and B3LYP (Tables S3 and S4, Supporting Information). Wildly deviating energy values between BP86 and B3LYP are in fact not unusual. This is why the combined spin state energies of the starting (**1**+**2**) and end (**3**+**4**) points differ considerably between the functionals (Figure 2), and this is also reflected in the energy differences of the intermediate states as well. However, the fact that BP86 gives a spin state ordering in agreement with experiments[18] and ab initio calculations[33] while most other functionals fail (including the popular B3LYP; see Table 1) makes the current case interesting from a theoretical point of view. These results indicate that caution may be needed when calculating Ni^{III}−peroxo/Ni^{II}−superoxo compounds, rather than indiscriminatingly relying on B3LYP. The fact that the B3LYP results show that the whole reaction is thermoneutral and therefore has no driving force is another indication that B3LYP may not be well suited for this particular reaction; experiments have indicated that the reverse reaction is not possible.[18] The bonding Ni 3d−O_2 π^* orbital in **1** containing one electron from each side coupled together may account for the electron count implying a Ni^{II}−superoxide configuration in calculations.[33] However, this results in a Mulliken spin density distribution of 1.08 and 0.10 (BP86 values) on Ni and O_2, respectively, pointing to a possible explanation to the experimentally determined Ni^{III}−peroxo assignment.

The calculations on the $O_2^{\bullet-}$ transfer reaction agree on the existence of a short-lived μ-1,2-O_2-bridged Ni−O−O−Mn intermediate. Orbital analysis and Mulliken spin density distributions imply either that an electron transfer from Mn^{II} has occurred at this stage in the case of BP86 and a septet ground state (i.e., Ni^{II}−peroxo−Mn^{III}) or that it is still a Ni^{II}−superoxo−Mn^{II} configuration in the case of B3LYP and a triplet ground state. The quintet state is excluded due to high energies in the second step, for both functionals. However, it remains to be verified if ^{3}**3** undergoes a spin relaxation to its low spin state (and thus to the overall quintet state) or not after the reaction is completed, as BP86 indicates. There is to date no experimental information regarding the spin state of **3** without any axial ligands attached, as is currently modeled. The experimental rate constant for the whole reaction is 0.2 M^{-1} s^{-1},[18] corresponding to a rate-limiting barrier of 13.6 kcal/mol converted through the Eyring equation. This value is however a free-energy value, done in an acetone solution at −50 °C because the reaction is otherwise too fast. It should also include the complexation energy and entropy due to loss of degrees of freedom, which are difficult to obtain theoretically. Our calculated low rate-limiting barriers for the reactions (5.0 and 4.4 kcal/mol for BP86 and B3LYP, respectively, excluding thermal effects and complexation energies) should therefore be qualitatively in agreement with the very fast reaction seen experimentally. On the basis of the above results, we predict a μ-1,2-O_2 bridge also in the case of the observed $O_2^{\bullet-}$ transfer from [(12- or 13-TMC)CoO_2]$^+$ to **2**[16] as the bridging mode seems to be more ligand- rather than metal-dependent.[22] Moreover, the current study characterizes for the first time an oxygen derived intermediate structure in a complete O_2 transfer

dx.doi.org/10.1021/jz501193k | J. Phys. Chem. Lett. 2014, 5, 2437−2442

reaction, and further studies are underway for other similar reactions.

METHODS

The calculations were done with the Gaussian 09 package.[36] A wide range of functionals and basis set combinations were tested for the current system, as described in the text. On the basis of those tests, the $O_2^{\bullet-}$ transfer reactions were geometry optimized using the BP86 functional (the Gaussian notation for this functional is BVP86, using VWN5 for the local correlation part) in combination with the SVP basis set. Energy evaluation results and Mulliken spin density distributions from both BP86/Def2-TZVPP//BP86/SVP and B3LYP/Def2-TZVPP//BP86/SVP levels are presented. Solvent effects (acetonitrile) were included using the CPCM scheme, even during the optimizations.[38,39] Zero-point energies, enthalpies, entropies, and dispersion effects were calculated at the BP86/SVP//BP86/SVP level but are reported only in the Supporting Information as their accuracy in solvent-optimized systems have been questioned (see the Methods section in the Supporting Information).[40]

ASSOCIATED CONTENT

Supporting Information

Full reference for ref 36, methodology discussions, calculated energies, Mulliken spin density distribution, and geometries. This material is available free of charge via the Internet at http://pubs.acs.org.

AUTHOR INFORMATION

Corresponding Author

*E-mail: wwnam@ewha.ac.kr.

Notes

The authors declare no competing financial interest.

ACKNOWLEDGMENTS

We thank Dr. Yong-Min Lee for helpful discussions. The research was supported by NRF of Korea (CRI NRF-2012R1A3A2048842 and GRL NRF-2010-00353 to W.N., R&D programs 14-BD-0403 and 2013K2A2A4000610 to J.C.), by the Ministry of Science, ICT & Future Planning of Korea (NRF 2013R1A1A2062737 to K.-B.C., KCRC 2011-0031992 to J.C.), and by the Israel Science Foundation (ISF 1183/13 to S.S.).

REFERENCES

(1) Klotz, I. M.; Kurtz, D. M., Jr. Metal−Dioxygen Complexes: A Perspective. *Chem. Rev.* **1994**, *94*, 567−568.
(2) Nam, W. Dioxygen Activation by Metalloenzymes and Models. *Acc. Chem. Res.* **2007**, *40*, 465−465.
(3) Decker, A.; Solomon, E. I. Dioxygen Activation by Copper, Heme and Non-Heme Iron Enzymes: Comparison of Electronic Structures and Reactivities. *Curr. Opin. Chem. Biol.* **2005**, *9*, 152−163.
(4) Hsia, C. C. W. Respiratory Function of Hemoglobin. *N. Engl. J. Med.* **1998**, *338*, 239−248.
(5) Springer, B. A.; Sligar, S. G.; Olson, J. S.; Phillips, G. N., Jr. Mechanisms of Ligand Recognition in Myoglobin. *Chem. Rev.* **1994**, *94*, 699−714.
(6) Ortiz de Montellano, P. R. *Cytochrome P450: Structure, Mechanism, and Biochemistry*, 3rd ed.; Springer: Berlin, Germany, 2005.
(7) Bollinger, J. M., Jr.; Price, J. C.; Hoffart, L. M.; Barr, E. W.; Krebs, C. Mechanism of Taurine: α-Ketoglutarate Dioxygenase (TauD) from Escherichia coli. *Eur. J. Inorg. Chem.* **2005**, *2005*, 4245−4254.
(8) Solomon, E. I.; Chen, P.; Metz, M.; Lee, S.-K.; Palmer, A. E. Oxygen Binding, Activation, and Reduction to Water by Copper Proteins. *Angew. Chem., Int. Ed.* **2001**, *40*, 4570−4590.
(9) Barondeau, D. P.; Kassmann, C. J.; Bruns, C. K.; Tainer, J. A.; Getzoff, E. D. Nickel Superoxide Dismutase Structure and Mechanism. *Biochemistry* **2004**, *43*, 8038−8047.
(10) Prabhakar, R.; Morokuma, K.; Musaev, D. G. A DFT Study of the Mechanism of Ni Superoxide Dismutase (NiSOD): Role of the Active Site Cysteine-6 Residue in the Oxidative Half-Reaction. *J. Comput. Chem.* **2006**, *27*, 1438−1445.
(11) Miriyala, S.; Spasojevic, I.; Tovmasyan, A.; Salvemini, D.; Vujaskovic, Z.; St. Clair, D.; Batinic-Haberle, I. Manganese Superoxide Dismutase, MnSOD and Its Mimics. *Biochim. Biophys. Acta* **2012**, *1822*, 794−814.
(12) Tainer, J. A.; Getzoff, E. D.; Richardson, J. S.; Richardson, D. C. Structure and Mechanism of Copper, Zinc Superoxide Dismutase. *Nature* **1983**, *306*, 284−287.
(13) Momenteau, M.; Reed, C. A. Synthetic Heme-Dioxygen Complexes. *Chem. Rev.* **1994**, *94*, 659−698.
(14) Hatcher, L. Q.; Karlin, K. D. Oxidant Types in Copper-Dioxygen Chemistry: The Ligand Coordination Defines the Cu_n-O_2 Structure and Subsequent Reactivity. *J. Biol. Inorg. Chem.* **2004**, *9*, 669−683.
(15) Bakac, A. Kinetic and Mechanistic Studies of the Reactions of Transition Metal-Activated Oxygen with Inorganic Substrates. *Coord. Chem. Rev.* **2006**, *250*, 2046−2058.
(16) Cho, J.; Sarangi, R.; Kang, H. Y.; Lee, J. Y.; Kubo, M.; Ogura, T.; Solomon, E. I.; Nam, W. Synthesis, Structural, and Spectroscopic Characterization and Reactivities of Mononuclear Cobalt(III)−Peroxo Complexes. *J. Am. Chem. Soc.* **2010**, *132*, 16977−16986.
(17) Kieber-Emmons, M. T.; Annaraj, J.; Seo, M. S.; Van Heuvelen, K. M.; Tosha, T.; Kitagawa, T.; Brunold, T. C.; Nam, W.; Riordan, C. G. Identification of an "End-on" Nickel−Superoxo Adduct, $[Ni(tmc)(O_2)]^+$. *J. Am. Chem. Soc.* **2006**, *128*, 14230−14231.
(18) Cho, J.; Sarangi, R.; Annaraj, J.; Kim, S. Y.; Kubo, M.; Ogura, T.; Solomon, E. I.; Nam, W. Geometric and Electronic Structure and Reactivity of a Mononuclear "Side-on" Nickel(III)−Peroxo Complex. *Nat. Chem.* **2009**, *1*, 568−572.
(19) Aboelella, N. W.; York, J. T.; Reynolds, A. M.; Fujita, K.; Kinsinger, C. R.; Cramer, C. J.; Riordan, C. G.; Tolman, W. B. Mixed Metal Bis(μ-Oxo) Complexes with $[CuM(\mu\text{-}O)_2]^{n+}$ (M = Ni(III) or Pd(II)) Cores. *Chem. Commun.* **2004**, No. No. 15, 1716−1717.
(20) Spencer, D. J. E.; Aboelella, N. W.; Reynolds, A. M.; Holland, P. L.; Tolman, W. B. β-Diketiminate Ligand Backbone Structural Effects on Cu(I)/O_2 Reactivity: Unique Copper−Superoxo and Bis(μ-oxo) Complexes. *J. Am. Chem. Soc.* **2002**, *124*, 2108−2109.
(21) Kieber-Emmons, M. T.; Schenker, R.; Yap, G. P. A.; Brunold, T. C.; Riordan, C. G. Spectroscopic Elucidation of a Peroxo $Ni_2(\mu\text{-}O_2)$ Intermediate Derived from a Nickel(I) Complex and Dioxygen. *Angew. Chem., Int. Ed.* **2004**, *43*, 6716−6718.
(22) Kieber-Emmons, M. T.; Riordan, C. G. Dioxygen Activation at Monovalent Nickel. *Acc. Chem. Res.* **2007**, *40*, 618−625.
(23) Kitajima, N.; Fujisawa, K.; Moro-oka, Y.; Toriumi, K. $\mu\text{-}\eta^2\text{:}\eta^2$-Peroxo Binuclear Copper Complex, $[Cu(HB(3,5\text{-}iPr_2pz)_3)]_2(O_2)$. *J. Am. Chem. Soc.* **1989**, *111*, 8975−8976.
(24) Kohn, W.; Sham, L. J. Self-Consistent Equations Including Exchange and Correlation Effects. *Phys. Rev.* **1965**, *140*, A1133−A1138.
(25) Latifi, R.; Tahsini, L.; Kumar, D.; Sastry, G. N.; Nam, W.; de Visser, S. P. Oxidative Properties of a Nonheme Ni(II)(O_2) Complex: Reactivity Patterns for C−H Activation, Aromatic Hydroxylation and Heteroatom Oxidation. *Chem. Commun.* **2011**, *47*, 10674−10676.
(26) Becke, A. D. Density-Functional Exchange-Energy Approximation with Correct Asymptotic Behavior. *Phys. Rev. A* **1988**, *38*, 3098−3100.
(27) Perdew, J. P. Density-Functional Approximation for the Correlation Energy of the Inhomogeneous Electron Gas. *Phys. Rev. B* **1986**, *33*, 8822−8824.

(28) Vosko, S. H.; Wilk, L.; Nusair, M. Accurate Spin-Dependent Electron Liquid Correlation Energies for Local Spin Density Calculations: A Critical Analysis. *Can. J. Phys.* **1980**, *58*, 1200−1211.
(29) Becke, A. D. A New Mixing of Hartree−Fock and Local Density-Functional Theories. *J. Chem. Phys.* **1993**, *98*, 1372−1377.
(30) Becke, A. D. Density-Functional Thermochemistry. III. The Role of Exact Exchange. *J. Chem. Phys.* **1993**, *98*, 5648−5652.
(31) Lee, C.; Yang, W.; Parr, R. G. Development of the Colle−Salvetti Correlation-Energy Formula into a Functional of the Electron Density. *Phys. Rev. B* **1988**, *37*, 785−789.
(32) Cho, J.; Kang, H. Y.; Liu, L. V.; Sarangi, R.; Solomon, E. I.; Nam, W. Mononuclear Nickel(II)−Superoxo and Nickel(III)−Peroxo Complexes Bearing a Common Macrocyclic TMC Ligand. *Chem. Sci.* **2013**, *4*, 1502−1508.
(33) Zapata-Rivera, J.; Caballol, R.; Calzado, C. J. The Role of Macrocyclic Ligands in the Peroxo/Superoxo Nature of Ni−O_2 Biomimetic Complexes. *J. Comput. Chem.* **2012**, *33*, 1407−1415.
(34) Olsen, J. The CASSCF Method: A Perspective and Commentary. *Int. J. Quantum Chem.* **2011**, *111*, 3267−3272.
(35) Seo, M. S.; Kim, J. Y.; Annaraj, J.; Kim, Y.; Lee, Y.-M.; Kim, S.-J.; Kim, J.; Nam, W. $[Mn(tmc)(O_2)]^+$: A Side-On Peroxido Manganese(III) Complex Bearing a Non-Heme Ligand. *Angew. Chem., Int. Ed.* **2007**, *46*, 377−380.
(36) Frisch, M. J.; Trucks, G. W.; Schlegel, H. B.; Scuseria, G. E.; Robb, M. A.; Cheeseman, J. R.; Scalmani, G.; Barone, V.; Mennucci, B.; Petersson, G. A.; et al. *Gaussian 09*, revisions B.01 & D.01; Gaussian, Inc.: Wallingford, CT, 2009.
(37) Cho, K.-B.; Kang, H.; Woo, J.; Park, Y. J.; Seo, M. S.; Cho, J.; Nam, W. Mechanistic Insights into the C−H Bond Activation of Hydrocarbons by Chromium(IV) Oxo and Chromium(III) Superoxo Complexes. *Inorg. Chem.* **2014**, *53*, 645−652.
(38) Cossi, M.; Rega, N.; Scalmani, G.; Barone, V. Energies, Structures, and Electronic Properties of Molecules in Solution with the C-PCM Solvation Model. *J. Comput. Chem.* **2003**, *24*, 669−681.
(39) Barone, V.; Cossi, M. Quantum Calculation of Molecular Energies and Energy Gradients in Solution by a Conductor Solvent Model. *J. Phys. Chem. A* **1998**, *102*, 1995−2001.
(40) Ho, J.; Klamt, A.; Coote, M. L. Comment on the Correct Use of Continuum Solvent Models. *J. Phys. Chem. A* **2010**, *114*, 13442−13444.